HHS Public Access

Author manuscript

Biomed Mater. Author manuscript; available in PMC 2018 April 28.

Published in final edited form as:

Biomed Mater. ; 12(2): 025021. doi:10.1088/1748-605X/aa6810.

Performance of laser sintered Ti-6Al-4V implants with bone-inspired porosity and micro/nanoscale surface roughness in the rabbit femur

David J. Cohen[a,†], **Alice Cheng**[b,c,†], **Kaan Sahingur**[a], **Ryan M. Clohessy**[a], **Louis B. Hopkins**[a], **Barbara D. Boyan**[a,b,*], and **Zvi Schwartz**[a,d]

[a]Department of Biomedical Engineering, Virginia Commonwealth University, Richmond, VA, USA

[b]Wallace H. Coulter Department of Biomedical Engineering at Georgia Tech and Emory University, Georgia Institute of Technology and Emory University, Atlanta, GA, USA

[c]Department of Biomedical Engineering, Peking University, Beijing, China

[d]Department of Periodontology, University of Texas Health Science Center at San Antonio, San Antonio, TX, USA

Abstract

Long term success of bone-interfacing implants remains a challenge in compromised patients and in areas of low bone quality. While surface roughness at the micro/nanoscale can promote osteogenesis, macro-scale porosity is important for promoting mechanical stability of the implant over time. Currently, machining techniques permit pores to be placed throughout the implant, but the pores are generally uniform in dimension. The advent of laser sintering provides a way to design and manufacture implants with specific porosity and variable dimensions at high resolution. This approach enables production of metal implants that mimic complex geometries found in biology. In this study, we used a rabbit femur model to compare osseointegration of laser sintered solid and porous implants. Ti-6Al-4V implants were laser sintered in a clinically relevant size and shape. One set of implants had a novel porosity based on human trabecular bone; both sets had grit-blasted/acid-etched surfaces. After characterization, implants were inserted transaxially into rabbit femora; mechanical testing, microCT and histomorphometry were conducted 10 weeks postoperatively. There were no differences in pull-out strength or bone-to-implant contact. However, both microCT and histomorphometry showed significantly higher new bone volume for porous compared to solid implants. Bone growth was observed into porous implant pores, especially near apical portions of the implant interfacing with cortical bone. These results show that laser sintered Ti-6Al-4V implants with micro/nanoscale surface roughness and trabecular bone-inspired porosity promote bone growth and may be used as a superior alternative to solid implants for bone-interfacing implants.

[*]Corresponding author: Barbara D. Boyan, PhD, School of Engineering, Virginia Commonwealth University, 601 West Main Street, Richmond, VA 23219, Telephone: 804-828-0190, Fax: 804-828-9866, bboyan@vcu.edu.

[†]These authors contributed equally to this manuscript.

Keywords

Additive manufacturing; orthopaedic implants; dental implants; osseointegration; animal models; surface topography

1. Introduction

The long term osseointegration of dental and orthopaedic implants continues to be a challenge, particularly for patients with poor bone quality. Success rates for titanium (Ti) and titanium-aluminum-vanadium (Ti-6Al-4V) dental implants can vary from over 90% in healthy patients to less than 70% in compromised patients [1]. The lifespan of many orthopaedic implants is limited to 15 years, requiring costly and potentially fatal revision procedures for continued functionality [2, 3]. In addition, an increasing life expectancy and demand for total joint replacements will require better performing implants with longer lifespans [4].

Osseointegration of implants can be affected by physical properties at the surface including chemistry, wettability and topography. Implants that are Ti based can directly integrate with bone. This is due in part to their passive TiO_2 layer that resists corrosion. Implants with surface micro-roughness show superior clinical performance compared to smooth implants [5]. In addition, increased wettability has been shown to increase the rate of osseointegration and implant mechanical stability in both animals and humans [6, 7]. Most recently, surfaces possessing hierarchical micro/nanoscale roughness are being explored and have been shown to enhance biological response compared to micro-roughness alone [8–11]. All these factors contribute to creating a desirable interface for cell attachment, osteoblast differentiation and ultimately bone formation for successful implant osseointegration.

Macro-scale properties such as porosity also play an important role in enhancing bone formation and osseointegration [12]. Laser sintered implants with through-pores and micro/nanoscale surface topography showed enhanced osseointegration and vertical bone growth in a rat calvarial bone onlay model as evidenced by increased pull-out values when compared to solid implants [13]. No differences in mechanical testing results or vertical bone ingrowth were observed between porous implants placed with or without the use of an osteoinductive bone graft, suggesting that implant surface and porosity alone were able to induce bone growth. This earlier study evaluated vertical growth of cortical bone, however, and did not consider the effects of porous implant design on trabecular bone, which is in contact with implants under many clinical conditions.

Porous implants have been introduced clinically in order to match the mechanical properties of bone and increase integration, but a clear consensus on the ideal properties of pores has not yet been reached [14]. Our approach has been to incorporate porosity inspired by nature, using human trabecular bone as the template. Previously, we showed that laser sintered Ti-6Al-4V constructs with trabecular bone-inspired porosity possess lower compressive moduli than solid implants and increase osteoblast differentiation of human mesenchymal stem cells (MSCs) and enhance osteoblast response in vitro [15, 16].

These results combined with *in vivo* studies demonstrating the ability of laser sintered implants to perform as well as implants manufactured with conventional techniques in animal models [17, 18], suggest that laser sintered implants with trabecular bone-inspired porosity may be superior to solid implants and enhance osseointegration in challenging clinical cases. While these results are promising, osseointegration of implants with trabecular bone-inspired porosity has not yet been analyzed in a clinically relevant orthopaedic or dental animal model. Therefore, the objective of this study was to evaluate and compare osseointegration of laser sintered Ti-6Al-4V implants with a solid or a trabecular bone-inspired porous exterior in a rabbit model that includes both cortical and cancellous bone. We hypothesized that laser sintered implants with a three-dimensional, trabecular porosity and a micro/nano-rough surface topography would increase new bone formation and enhance osseointegration compared to solid sintered implants with the same surface roughness.

2. Methods

2.1. Implant manufacturing

Implants were manufactured from Ti-6Al-4V powder with laser sintering using processing parameters described previously (EOS GmbH, Kralling, Germany) [15]. Implants were 3.8mm in diameter and 8mm in length. Both solid and porous implants possessed similar internal abutment connections and only differed in their solid or porous exterior. Porous implants were designed from a “medium porosity, high resolution” microCT template of human femoral trabecular bone [15]. After manufacturing, implants were blasted with calcium phosphate particles and pickled to remove impurities, resulting in surface micro/nanoscale roughness [15]. All implants were sterilized with gamma irradiation prior to characterization and implantation.

2.2. Implant characterization

2.2.1. Scanning electron microscopy—Scanning electron microscopy (SEM, Zeiss AURIGA, Oberkochen, Germany) was used to qualitatively evaluate implant macrostructure and surface roughness. Implants were secured on stubs with carbon tape and imaged with an accelerating voltage of 4kV, 30μm aperture and working distance of between 4-6mm. An SE2 detector was used to image samples.

2.2.2. Laser confocal microscopy—Laser confocal microscopy (LCM, Zeiss LSM 710) was used to quantitatively evaluate surface micro-roughness [15]. A Plan Apochromat 40×/0.95 Corr M27 objective was used with an additional 5× optical zoom. Scan areas were 42.5μm × 42.5μm and imaged using the 405nm laser in reflection mode, with a 0.04μm pixel size and 1.60μs pixel dwell time. Z-stacks were performed using a step size of 1μm. Primary average roughness (Ra) and peak to valley roughness (Rz) were averaged over 3 scans per implant, with two implants per group (total n=6).

2.2.3. Micro-computed tomography—Micro-computed tomography (microCT, SkyScan 1173, Bruker, Kontich, Belgium) was used to evaluate implant porosity. A 0.25mm brass filter was used with a voltage of 120kV, current of 60μA, exposure of 300ms, pixel

size of 40μm and rotation step of 0.2°. Scans were reconstructed in NRecon (Bruker) and analyzed in CT-Analyser (Bruker). A cylindrical volume of interest (VOI) was defined for only the lower half of implants to avoid analysis of the internal screw. This VOI was binarized and then thresholded to determine total implant porosity.

2.2.4. X-ray photoelectron spectroscopy (XPS)—Surface chemistry of implants was evaluated with XPS (ThermoFisher ESCAlab 250, Thermo Scientific, Waltham, Massachusetts, USA). Averages were taken over two survey scans per 500μm spot, using an XR5 gun and Al Kα x-ray source at 15kV. Scans were taken with a 20ms dwell time and 1eV step size. Four locations per implant for two solid and two porous implants (n=8) were analyzed.

2.2.5. Contact angle—Surface wettability of solid implants was evaluated by sessile drop contact angle analysis (Raméhart Instrument Co, Succasunna, New Jersey, USA). A 1μL drop of distilled water was placed on the body of implants and analyzed with DROPImage software (Ramé-hart Instrument Co). Left and right contact angles were averaged every 5 seconds for 20 seconds per drop, with 4 drops placed per implant for two implants (n=8).

2.3 Surgical procedure

A schematic of the surgical procedure and harvest is provided in Figure 1A. Male New Zealand White rabbits 13-16 weeks of age (7.0-7.9 pounds, late adolescent) were obtained from Robinson Services Inc. (Mocksville, North Carolina, USA). Anesthesia was induced with an intramuscular injection of 35 mg/kg ketamine and 5 mg/kg xylazine, followed by a subcutaneous injection of 0.12 mg/kg buprenorphine SRLab for post-operative analgesia. Anesthesia was maintained using isoflurane gas delivered by v-gel supraglottic airway in 3-4% oxygen to effect. The greater trochanter of the femur was palpated and a 5cm vertical incision was made distal to this landmark. The muscles were separated and the posterior surface of the proximal femur was localized. The periosteum was elevated and increasing drill bit diameters were used (1.9, 2.0, 2.5, 3.2, 3.65, and 3.8mm) to create a 3.8mm defect by drilling transaxially through the cortical and cancellous portions of the femur to a depth of 8mm. Solid or porous implants were press fit into the defects flush with the cortical surface, and capped with a cover screw. The periosteum and muscle were reapproximated, and the skin incision was closed with a running technique. Rabbits were euthanized after 10 weeks with a 0.22ml/kg intravenous injection of euthanasia solution, and the implants were harvested for pull-out testing (n=10) or microCT and histological analysis (n=10). Approval was obtained from the Institutional Animal Care and Use Committee at Virginia Commonwealth University. All experiments were carried out in accordance with approved procedures and reported according to ARRIVE guidelines [19].

2.4 Tissue analysis

2.4.1. Mechanical testing—Pull out testing was performed using a MTS materials test system (MTS Insight 30; MTS Systems Corp., Eden Prairie, MN, USA) as published previously [13]. The femur specimen was fixed in a custom fabricated test device with the implant aligned to the testing machine axis to ensure that no bending moment was created during the test. A custom abutment fabricated by AB Dental (Ashdod, Israel) was joined to

the implant and then pulled at a crosshead speed of 10 mm/min. Axial pull-out strengths were recorded and the load was monitored for force at failure (N) on nineteen implants (11 solid, 8 porous).

2.4.2. MicroCT—Bone growth in and around implants was evaluated by microCT (Figure 1B). Fixed samples were imaged with a voltage of 130 kV and current of 60μA. High resolution scans were conducted using a 10μm pixel size, 1500ms exposure time and 0.4° rotation step. After reconstruction, shrink-wrapping was performed to isolate an initial VOI containing the implant. The VOI was dilated 10 pixels (100 μm) to account for new bone formed around the outside of implants and in order to provide a comparison between solid and porous implants. This final VOI was thresholded to subtract the implant, leaving only the bone remaining. The VOI was reloaded and the bone was thresholded, binarized and quantified as the total bone volume. Total bone as a percentage of VOI was calculated by dividing the total bone volume by the final VOI. Total bone as a percentage of pore volume was calculated by diving the total bone volume by the pore volume from control implants as described above. Apical bone volume values were calculated by restricting the VOI to only the lower half of implants below the internal hex connector.

2.4.3. Histomorphometry—Samples were commercially processed (Histion, Everett, WA). Femurs were embedded in methyl methacrylate, and one ground section from each specimen was stained with Stevenel's blue/van Gieson. Sections were imaged with an AxioCam MRc5 camera and Axio Observer Z.1 and analyzed using ZEN 2012 Blue Edition software (Carl Zeiss Microscopy, Oberkochen, Germany).

The total bone-to-implant contact (BIC) was determined by dividing the length of bone touching the exterior of the implant by the total length of the exterior of the implant. The cortical region was set as the region from the two uppermost points of the implant, one on either side of the implant, down 2mm along the exterior of the implant. The total base length was calculated by finding the length of the horizontal component of the implant at its bottom. Some samples maintained an unbroken base, which resulted in a base measurement across the full length. Because porous implants did not retain a solid base across the full length of the implant, the implant base of these samples was calculated as the combined lengths of the fragmented pieces that appeared at the bottom of the implant closest to the bone. The BIC was calculated based on the bone touching these fragments.

The total bone ingrowth of the implant was calculated by dividing the total area of bone within the implant by the total area within the implant without bone (Figure 1C). A horizontal line was drawn across the two highest points on either side of the implant, the total area of the bone in the implant was was analyzed within these boundaries.

2.5. Statistics

Average and standard error of the mean values are presented for all analyses. Comparisons between solid and porous implants were made using Student's unpaired t-test, with $p<0.05$ indicating significance.

3. Results

3.1. Implant characterization

SEM images were taken of implant macrostructure and surface roughness (Figure 2). Solid and porous implants were manufactured with the same dimensions. After surface processing, roughness at the microscale and nanoscale was present and similar on both solid and porous implants. Average and peak to valley surface micro-roughness were quantitatively evaluated by LCM; these values were not statistically different between solid and porous implants (Table 1). MicroCT revealed that porous implants possessed a total and open porosity of 68.6% ± 0.8%. XPS analysis of surface chemistry showed mostly O and C present on implant surfaces, with smaller amounts of Ti, N, Ca, Al and Na also present (Table 2). Contact angle of solid implants was 85°±11°.

3.2. Mechanical testing

Mechanical pull-out testing values for solid and porous implants at 10 weeks postoperatively were 441.2±64.0 N and 501.5 ± 47.6 N, respectively (Figure 3A). These values were not significantly different. SEM images of the surface (Figure 3B) and microCT reconstructed (Figure 3C) images of implants after mechanical testing showed bone formation on both solid and porous implants. Bone was also observed in pores of porous implants.

3.3. MicroCT

Axial and sagittal microCT reconstructions of solid and porous implants show bone growth around both implant groups (Figure 4). A view of the implant alone, bone around the implant a merged view show differences in bone growth around solid and porous implants. While mostly solid bone growth was achieved around solid implants, an interconnected network of trabecular-like bone was observed around and penetrating through porous implants.

MicroCT 3D reconstructions of implants in femurs showed bone formation around both solid and porous implants (Figure 5A). While dense bone formed around the outer cortex of solid implants, a porous bone network penetrated and formed throughout porous implants. Total bone volume within a VOI around porous implants was 20.7±1.2% of the entire implant volume, which was significantly higher than the 14.8±0.7% for solid implants (Figure 5B, Table 3). When isolated to just the apical portion of the implant, the percentage of bone volume over implant volume was 17.9±1.8% (Figure 5C). This value was also significantly higher than the percent of bone analyzed within the same VOI for solid implants, which was 4.6±0.3%.

3.4. Histomorphometry

Histological sections of solid (Figure 6A) and porous (Figures 6B) implants provide a more detailed view of bone growth around implants. Bone was observed interfacing along the body of solid implants, while bone was observed both around and inside pores of porous implants. Total BIC calculated the perimeter was not significantly different between solid and porous implants (Figure 6C). Total bone area within a fixed VOI containing the entire implant was significantly higher for porous compared to solid implants (Figure 6D). Bone

area calculated within a fixed VOI near the apex of implants was also greater for porous compared to solid implants (Figure 6E).

4. Discussion

Additive manufacturing has shown great potential in the field of biomaterials, with laser sintering of Ti-6Al-4V already being implemented for bone-interfacing implants. However, in many cases, postbuild surface modifications have not been used to enhance osseointegration. In the present study, the outer surface of the implant was treated to have microscale and nanoscale roughness similar to surface modifications shown to enhance osteoblast differentiation of MSCs and osteoblasts in vitro [16, 18]. While the line-of-sight blasting we used could not penetrate into construct pores, surface modification by acid etching combined with macro-porosity provided by the trabeculae, was able to increase markers for osteoblast differentiation [16]. Our results using the rabbit femoral bone model indicate that the presence of the trabecular bone-inspired porosity together with the nanorough surface generated by acid etching supported increased bone formation compared to solid laser sintered implants with comparable micro/nanoscale roughness on the exterior surface.

Characterization of the implants showed that the physical and chemical properties of the exterior implant surface (Figure 2, Tables 1 and 2) were comparable to previously manufactured constructs used for *in vitro* studies [15]. The implants used in the present study had a higher total porosity than those we have used previously. This may be attributed to the use of a different VOI size and location analyzed in our implant geometry compared to our previous construct geometry, although pores were interconnected for both constructs. Our results confirmed that surface roughness was comparable across solid and porous implants, showing the versatility of surface treatments for different construct geometries.

Our group has shown that laser sintered Ti-6Al-4V solid implants placed in rabbit tibia cortical bone perform better than traditional implants manufactured with computer numerical control (CNC) [17]. We have also shown in previous studies that use of an osteoinductive agent (DBX, Musculoskeletal Transplant Foundation, Edison, New Jersey, USA) on rat calvaria did not alter the mechanical pull-out strength or new bone volume analyzed by microCT of porous laser sintered implants at 10 weeks postoperatively [13]. However, histological analysis showed 16% of the implant pores still contained DBX, suggesting the potential for enhanced bone growth over time in DBX-treated sites. We did not use DBX or another osteoinductive or osteogenic agent in this study in order to evaluate the comparative effects of solid and 3D porous implants. However, we suggest that use of a bone graft substitute should still be considered for clinical cases requiring large volumes of new bone.

Optimal pore size for osseointegration may vary with time, implant location, and surface treatment. A study comparing pore diameters of Ti implants in the rabbit tibia concluded that a 600μm pore diameter resulted in the most bone ingrowth and bone-material fixation compared to implants with 300μm and 900μm diameter pores over the 8 weeks of the experiment [20]. A study in the rabbit calvaria showed greater bone ingrowth into Ti

scaffolds with a maximum pore size of 600μm after 3 weeks, while implants with a maximum pore size of 100μm showed superior bone growth after 20 weeks [21]. In vitro data using 3D Ti mesh scaffolds suggest that bone growth and remodeling within the pores occur in cycles [22]. Thus, as new bone forms and remodels, changes will occur around the implant microenvironment that affect the rate and extent of bone formation, and these are influenced by the physical properties of the implant.

While our study suggests that additively manufactured implants with trabecular bone-inspired porosity can achieve superior osseointegration to solid implants (Table 3, Figures 3B, 5B and 6D), there are still limitations to our animal model and analysis. We chose the rabbit femur for implant placement because it better mimics the clinical placement of a dental or orthopaedic implant through both cortical and trabecular bone. This model is also more relevant than the calvarial bone onlay model, providing the ability to evaluate response to an implant size that could be used clinically. While vertical cortical bone formation had been previously observed in the cranial bone onlay model in rats, it was unclear how osseointegration would occur horizontally within trabecular bone [13]. For orthopaedic implants and for dental implant placement in the mandible, the ratio of cortical to cancellous bone contributes to primary stability and long term success [23, 24]. Our rabbit femoral implant model does not account for uniaxial mechanical loading, which is a major consideration when placing dental implants. Reports also indicate that bone remodeling in the mandible occurs more rapidly than in the femur, with distinct regeneration properties [25]. This may be due to mechanical forces experienced by the implant, as well as a different local microenvironment or system effects induced by implantation.

In addition, solid and porous implants used in this study both possessed a solid portion at the top of the implant for internal screw fixation (Figure 2). Because implants were inserted transaxially into the femur, the cortical shell came into contact with both the solid and porous portions of the porous implant. Thus, pull-out testing could not completely isolate the effects of a porous implant on mechanical strength (Figure 3A). Analysis of apical portions of implants in both groups via microCT (Figure 5) and histology (Figure 6) show that more bone is present in and around porous compared to solid implants, suggesting that mechanical strength is enhanced in porous areas.

Finally, this study only evaluated osseointegration of implants at one time point, 10 weeks after implantation. Previous studies have shown differences in bone healing around hydroxyapatite implants placed in rabbits up to 6 months after implantation [26]. Work from our group has also shown varied response to additively manufactured implants at 5 weeks compared to 10 weeks [13]. It may be possible that differences in healing occurred at an earlier time point, but stabilized for both implants after 10 weeks.

Not only did new cortical and trabecular bone form in porous implants and around both solid and porous implants, but the presence of new bone was also observed above and covering the implant. This was particularly obvious in histological sections (Figure 6A-B), which showed another layer of trabecular bone, marrow and cortical bone above the originally existing cortical bone. Previous studies have observed similar vertical bone growth along titanium implants placed in rabbit mandibles [27, 28]. However, the implants were placed

with at least 2mm exposed above the mandible to support supracrestal bone formation. In contrast, we observed vertical bone growth in this study over the implant and cover screw, without a physical implant presence to guide bone formation.

This phenomenon was also distinctly different than a bony callus, which has shown to result in cortical union by day 28 after fracture in the rabbit tibia [29]. The presence of an additional cortical and cancellous bone layer above the implant in our study after 10 weeks indicates that the bone was no longer in the callus stage of healing. Early studies of porous-coated intramedullary implants placed in beagle femurs showed that cortical bone formation occurred near the endosteal cortex, but also when placed up to 2mm away from the endosteum [30]. While multipotent stem cells and progenitor cells may contribute to trabecular bone formation within the medullary canal, our results suggest the cortical bone formation may first be influenced by cells from the endosteal cortex. This corroborates other findings that suggest cortical bone contributes to distant osteogenesis [31].

5. Conclusions

Porous Ti-6Al-4V constructs with surface roughness and bio-inspired porosity have shown enhanced cell response and mineralization *in vitro*. In this study, we observe osseointegration of these implants in a clinically relevant size with the rabbit femur. While both solid and porous implants were osseointegrated, trabecular bone-inspired porous implants allowed significantly more bone growth in some applications. This study suggests that additive manufacturing of porous Ti-6Al-4V implants may enhance osseointegration clinically compared to solid implants, and may be used to improve long term clinical outcomes.

Acknowledgments

This research was supported in part by AB Dental (Ashdod, Israel), which also generously manufactured the implants for this study. Research reported in this publication was also supported by the National Institute of Arthritis and Musculoskeletal and Skin Diseases of the National Institutes of Health under Award Number AR052102. The content is solely the responsibility of the authors and does not necessarily represent the official views of the National Institutes of Health. BDB is a paid consultant for Titan Spine LLC (Mequon, Wisconsin, USA) and unpaid consultant for Institut Straumann AG (Basel, Switzerland). ZS is a paid consultant for AB Dental.

References

1. Moy PK, Medina D, Shetty V, Aghaloo TL. Dental implant failure rates and associated risk factors. Int J Oral Maxillofac Implants. 2005; 20:569–77. [PubMed: 16161741]
2. Geetha M, Singh AK, Asokamani R, Gogia AK. Ti based biomaterials, the ultimate choice for orthopaedic implants – A review. Prog Mater Sci. 2009; 54:397–425.
3. Mahomed NN, Barrett JA, Katz JN, Phillips CB, Losina E, Lew RA, et al. Rates and outcomes of primary and revision Total hip replacement in the United States Medicare population. J Bone Joint Surg Am. 2003; 85:27–32. [PubMed: 12533568]
4. Iorio R, Robb WJ, Healy WL, Berry DJ, Hozack WJ, Kyle RF, et al. Orthopaedic surgeon workforce and volume assessment for total hip and knee replacement in the United States: Preparing for an epidemic. J Bone Joint Surg Am. 2008; 90:1598–605. [PubMed: 18594111]
5. Buser D, Nydegger T, Oxland T, Cochran DL, Schenk RK, Hirt HP, et al. Interface shear strength of titanium implants with a sandblasted and acid-etched surface: a biomechanical study in the maxilla of miniature pigs. Journal of biomedical materials research. 1999; 45:75–83. [PubMed: 10397960]

6. Gittens RA, Scheideler L, Rupp F, Hyzy SL, Geis-Gerstorfer J, Schwartz Z, et al. A review on the wettability of dental implant surfaces II: Biological and clinical aspects. Acta Biomater. 2014; 10:2907–18. [PubMed: 24709541]
7. Buser D, Broggini N, Wieland M, Schenk RK, Denzer AJ, Cochran DL, et al. Enhanced bone apposition to a chemically modified SLA titanium surface. Journal of dental research. 2004; 83:529–33. [PubMed: 15218041]
8. Gittens RA, McLachlan T, Olivares-Navarrete R, Cai Y, Berner S, Tannenbaum R, et al. The effects of combined micron-/submicron-scale surface roughness and nanoscale features on cell proliferation and differentiation. Biomaterials. 2011; 32:3395–403. [PubMed: 21310480]
9. Gittens RA, Olivares-Navarrete R, Cheng A, Anderson DM, McLachlan T, Stephan I, et al. The roles of titanium surface micro/nanotopography and wettability on the differential response of human osteoblast lineage cells. Acta Biomater. 2013; 9:6268–77. [PubMed: 23232211]
10. Gittens RA, Olivares-Navarrete R, McLachlan T, Cai Y, Hyzy SL, Schneider JM, et al. Differential responses of osteoblast lineage cells to nanotopographically-modified, microroughened titanium–aluminum–vanadium alloy surfaces. Biomaterials. 2012; 33:8986–94. [PubMed: 22989383]
11. Olivares-Navarrete R, Hyzy SL, Slosar PJ, Schneider JM, Schwartz Z, Boyan BD. Implant materials generate different peri-implant inflammatory factors: poly-ether-ether-ketone promotes fibrosis and microtextured titanium promotes osteogenic factors. Spine. 2015; 40:399–404. [PubMed: 25584952]
12. Karageorgiou V, Kaplan D. Porosity of 3D biomaterial scaffolds and osteogenesis. Biomaterials. 2005; 26:5474–91. [PubMed: 15860204]
13. Cohen DJ, Cheng A, Kahn A, Aviram M, Whitehead AJ, Hyzy SL, et al. Novel osteogenic Ti-6Al-4V device for restoration of dental function In patients with large bone deficiencies: Design, development and implementation. Sci Rep. 2016; (6):20493. [PubMed: 26854193]
14. Challis VJ, Roberts AP, Grotowski JF, Zhang L-C, Sercombe TB. Prototypes for bone implant scaffolds designed via topology optimization and manufactured by solid freeform fabrication. Adv Eng Mater. 2010; 12:1106–10.
15. Cheng A, Humayun A, Boyan BD, Schwartz Z. Enhanced osteoblast response to porosity and resolution of additively manufactured Ti-6Al-4V constructs with trabeculae-inspired porosity. 3D Print Addit Manuf. 2016; 3:10–21. [PubMed: 28804735]
16. Cheng A, Humayun A, Cohen DJ, Boyan BD, Schwartz Z. Additively manufactured 3D porous Ti-6Al-4V constructs mimic trabecular bone structure and regulate osteoblast proliferation, differentiation and local factor production in a porosity and surface roughness dependent manner. Biofabrication. 2014; 6:045007. [PubMed: 25287305]
17. Hyzy SL, Cheng A, Cohen DJ, Yatzkaier G, Whitehead AJ, Clohessy RM, et al. Novel hydrophilic nanostructured microtexture on direct metal laser sintered Ti-6Al-4V surfaces enhances osteoblast response in vitro and osseointegration in a rabbit model. J Biomed Mater Res A. 2016; 104:2086–98. [PubMed: 27086616]
18. Cheng A, Cohen DJ, Boyan BD, Schwartz Z. Laser sintered constructs with bio-inspired porosity and surface micro/nano roughness enhance mesenchymal stem cell differentiation and matrix mineralization in vitro. Calcif Tissue Int. 2016 (In press).
19. Kilkenny C, Browne W, Cuthill IC, Emerson M, Altman DG. Animal research: Reporting in vivo experiments: The ARRIVE guidelines. Br J Pharmacol. 2010; 160:1577–9. [PubMed: 20649561]
20. Taniguchi N, Fujibayashi S, Takemoto M, Sasaki K, Otsuki B, Nakamura T, et al. Effect of pore size on bone ingrowth into porous titanium implants fabricated by additive manufacturing: An in vivo experiment. Mater Sci Eng C Mater Biol Appl. 2016; 59:690–701. [PubMed: 26652423]
21. Prananingrum W, Naito Y, Galli S, Bae J, Sekine K, Hamada K, et al. Bone ingrowth of various porous titanium scaffolds produced by a moldless and space holder technique: an in vivo study in rabbits. Biomed Mater. 2016; (11):015012.
22. Wang X, Schwartz Z, Gittens RA, Cheng A, Olivares-Navarrete R, Chen H, et al. Role of integrin α2β1 in mediating osteoblastic differentiation on three-dimensional titanium scaffolds with submicron-scale texture. J Biomed Mater Res A. 2015; 103:1907–18. [PubMed: 25203434]
23. Sakka S, Coulthard P. Bone quality: A reality for the process of osseointegration. Implant Dent. 2009; 18:480–5. [PubMed: 20009601]

24. Miyamoto I, Tsuboi Y, Wada E, Suwa H, Iizuka T. Influence of cortical bone thickness and implant length on implant stability at the time of surgery—clinical, prospective, biomechanical, and imaging study. Bone. 2005; 37:776–80. [PubMed: 16154396]

25. Matsuura T, Tokutomi K, Sasaki M, Katafuchi M, Mizumachi E, Sato H. Distinct Characteristics of Mandibular Bone Collagen Relative to Long Bone Collagen: Relevance to Clinical Dentistry. Biomed Res Int. 2014; 2014:9.

26. Eggli PS, Muller W, Schenk RK. Porous hydroxyapatite and tricalcium phosphate cylinders with two different pore size ranges implanted in the cancellous bone of rabbits. A comparative histomorphometric and histologic study of bony ingrowth and implant substitution. Clin Orthop Relat Res. 1988:127–38.

27. Karl M, Freilich M, Wen B, Wei M, Shafer D, Kuhn L. Guided vertical bone regeneration by means of roughened and alkaline treated titanium implant surfaces. J Dent Implantol. 2011; 27:145–57.

28. Schiegnitz E, Palarie V, Nacu V, Al-Nawas B, Kammerer PW. Vertical osteoconductive characteristics of titanium implants with calcium-phosphate-coated surfaces - a pilot study in rabbits. Clin Implant Dent Relat Res. 2014; 16:194–201. [PubMed: 23675992]

29. Bax EB, Wozney MJ, Ashhurst ED. Bone morphogenetic protein-2 increases the rate of callus formation after fracture of the rabbit tibia. Calcif Tissue Int. 2014; 65:83–9.

30. Bobyn JD, Pilliar RM, Cameron HU, Weatherly GC. Osteogenic phenomena across endosteal bone-implant spaces with porous surfaced intramedullary implants. Acta Orthop Scand. 1981; 52:145–53. [PubMed: 7246092]

31. Davies JE. Understanding peri-implant endosseous healing. J Dent Educ. 2003; 67:932–49. [PubMed: 12959168]

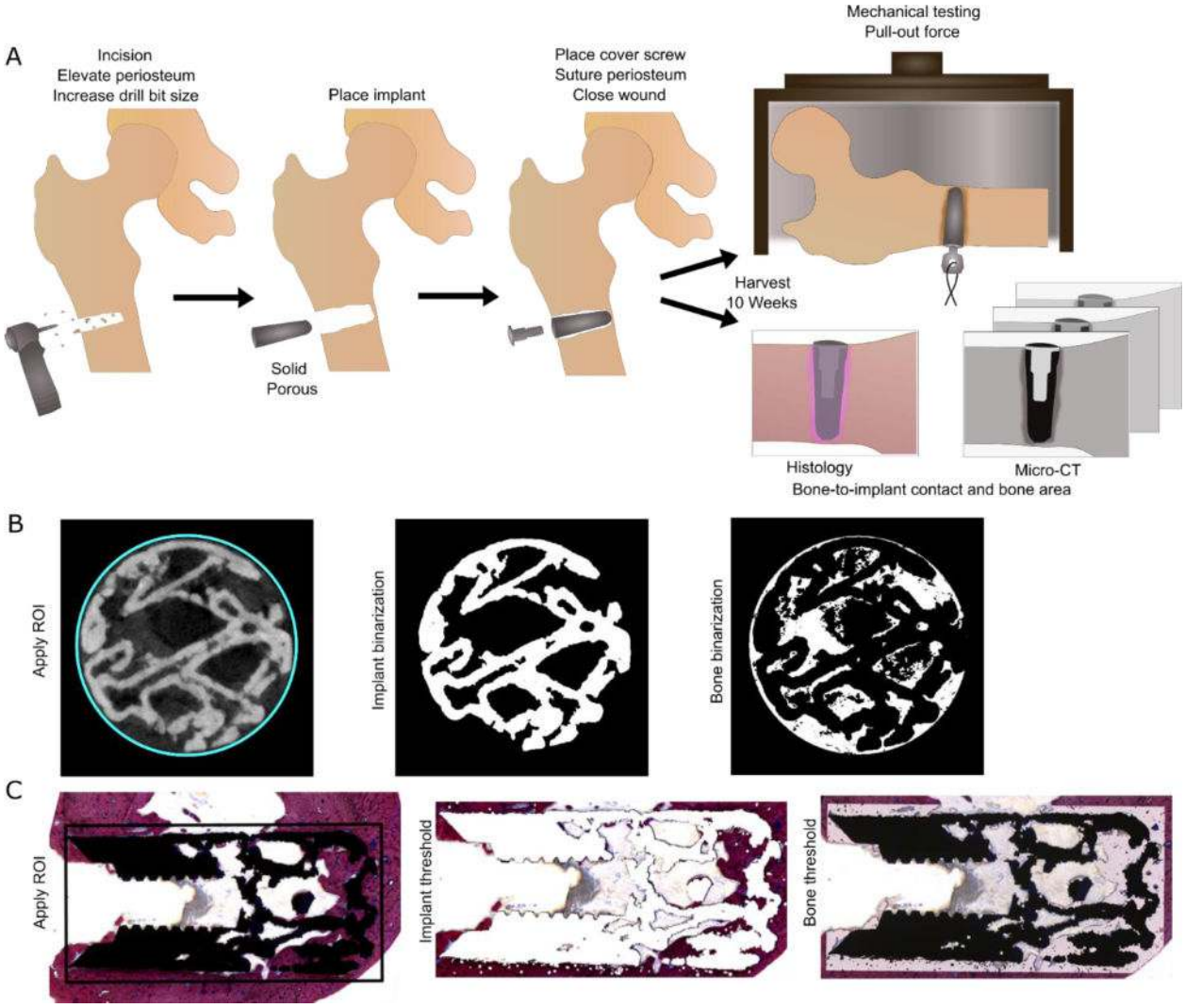

Figure 1.

Surgery schematic (A). After incision at the femur, the periosteum was lifted and increasing drill bit diameters were used to drill transaxially into the femur. Solid or porous implants were placed and capped with a cover screw. The periosteum and skin was sutured closed. Rabbits were harvested after 10 weeks. One group was used for pull-out testing, while the second group was used for microCT and histological analysis. MicroCT (B) and histological (C) methods for bone volume analysis.

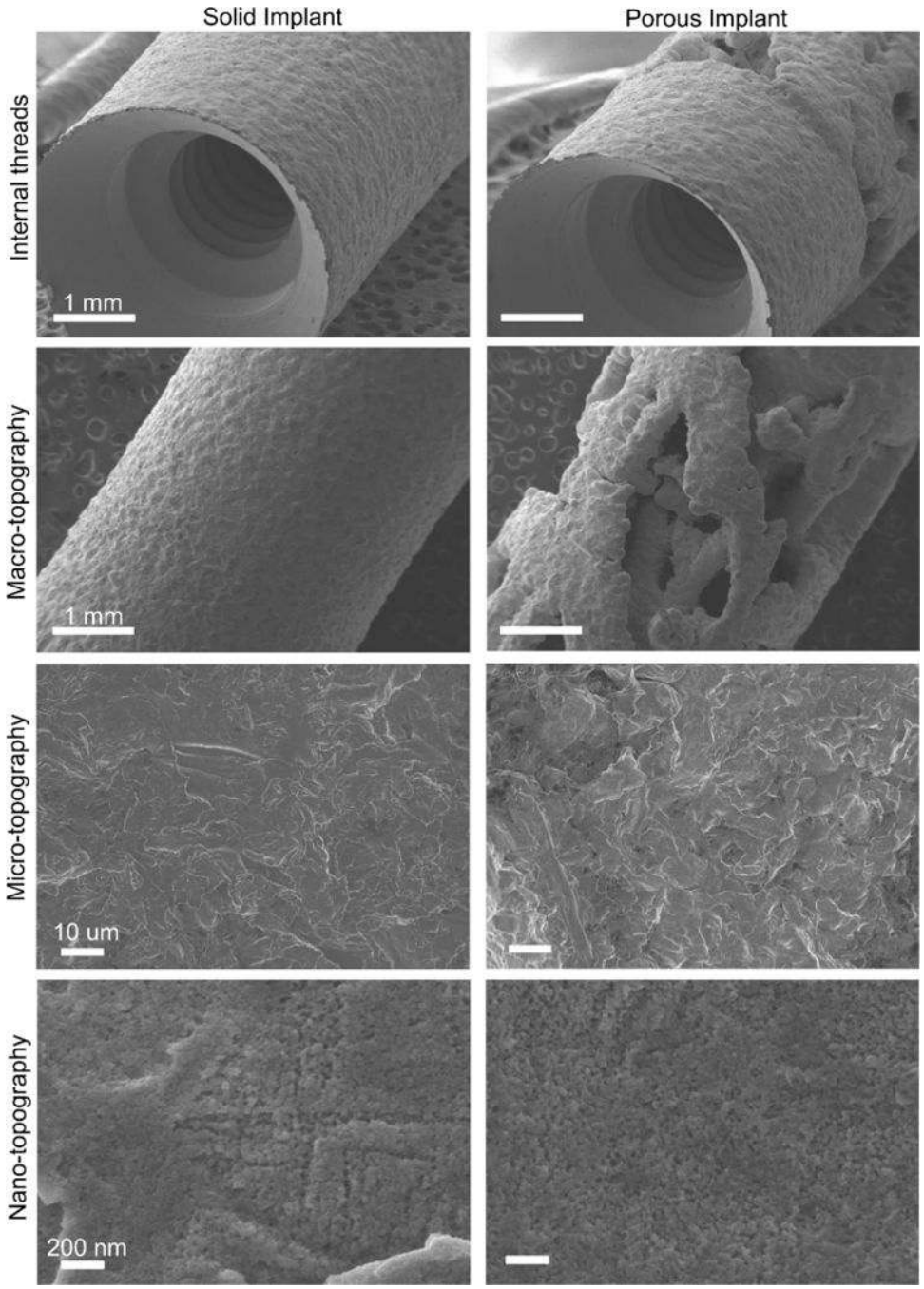

Figure 2.

Scanning electron micrographs of solid (left) and porous (right) implants showing the internal threads and top solid portions of both implants (top panel), macro- (second panel), micro- (third panel) and nano-scale topography (bottom panel) after manufacturing and surface processing.

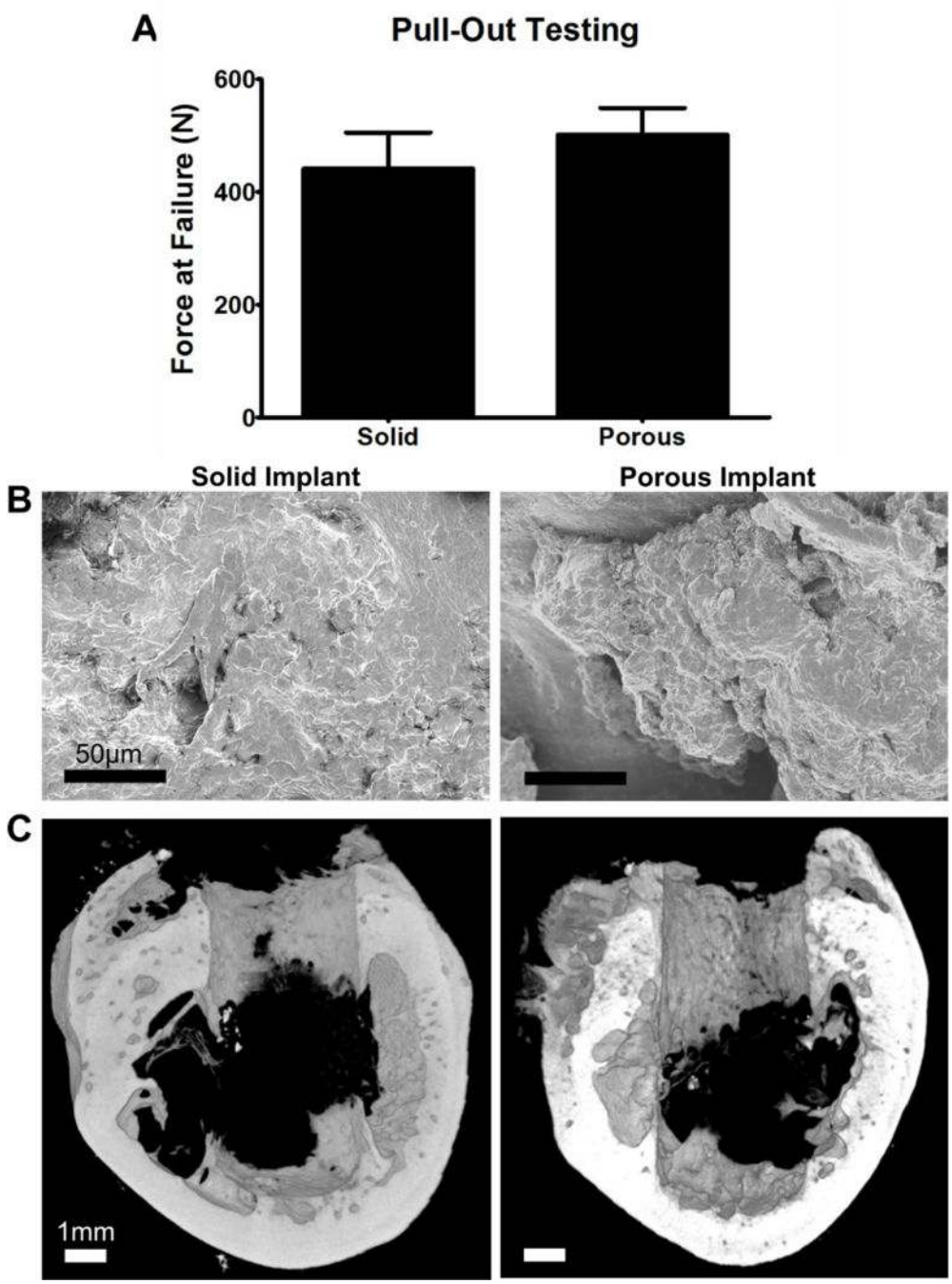

Figure 3.

Pull-out testing force at failure (A); scanning electron micrographs of implants showing little bone on solid implants but the presence of a larger volume of bone adjacent to porous implants (B); and microCT reconstructions (C) of after the implant site after mechanical testing.

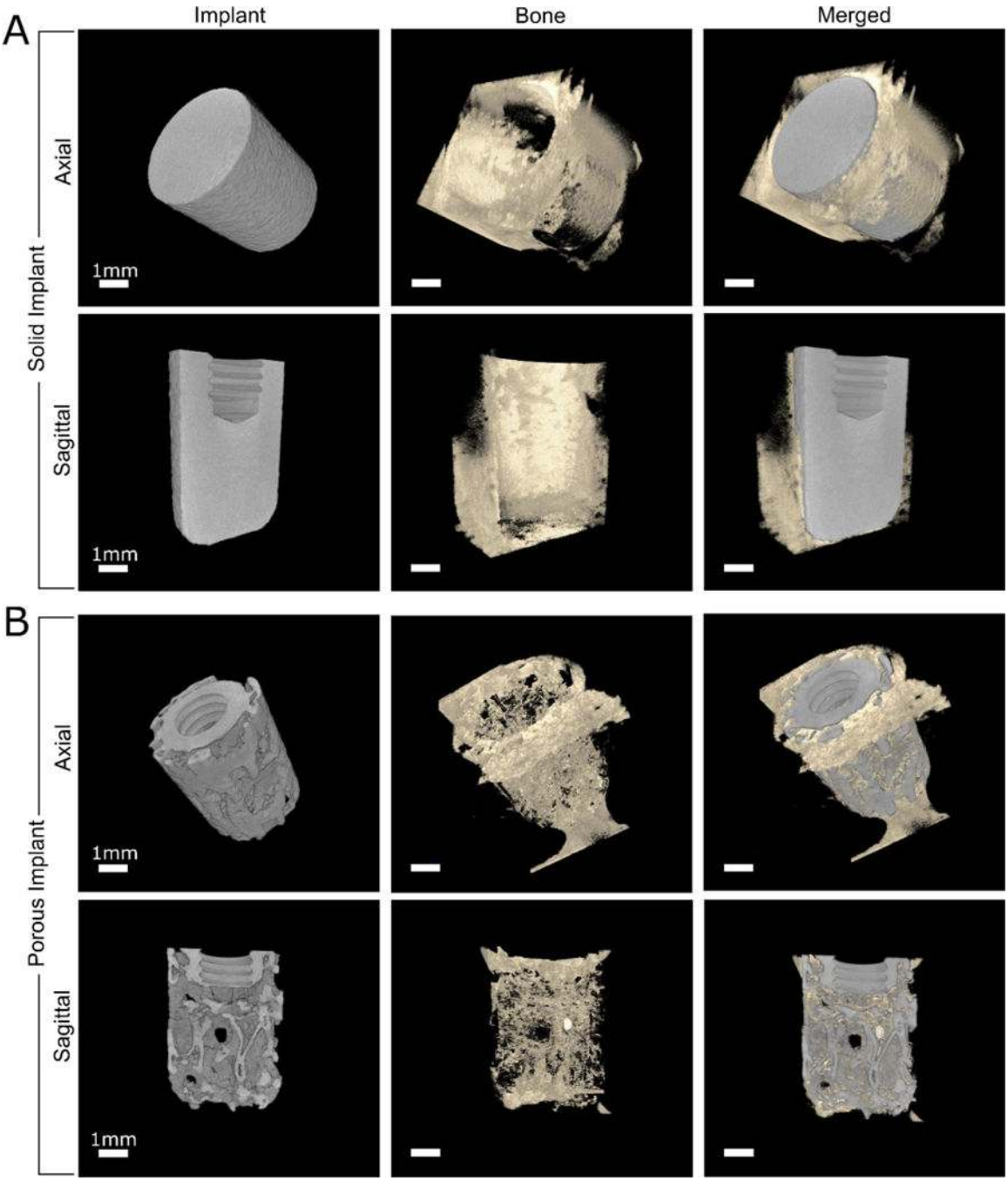

Figure 4.

MicroCT three-dimensional reconstructions of bone surrounding solid implants (A) and bone volume penetration in porous implants (B) after 10 weeks in rabbit femurs. For each implant group, top panel shows axial cross section and bottom panel shows sagittal cross section.

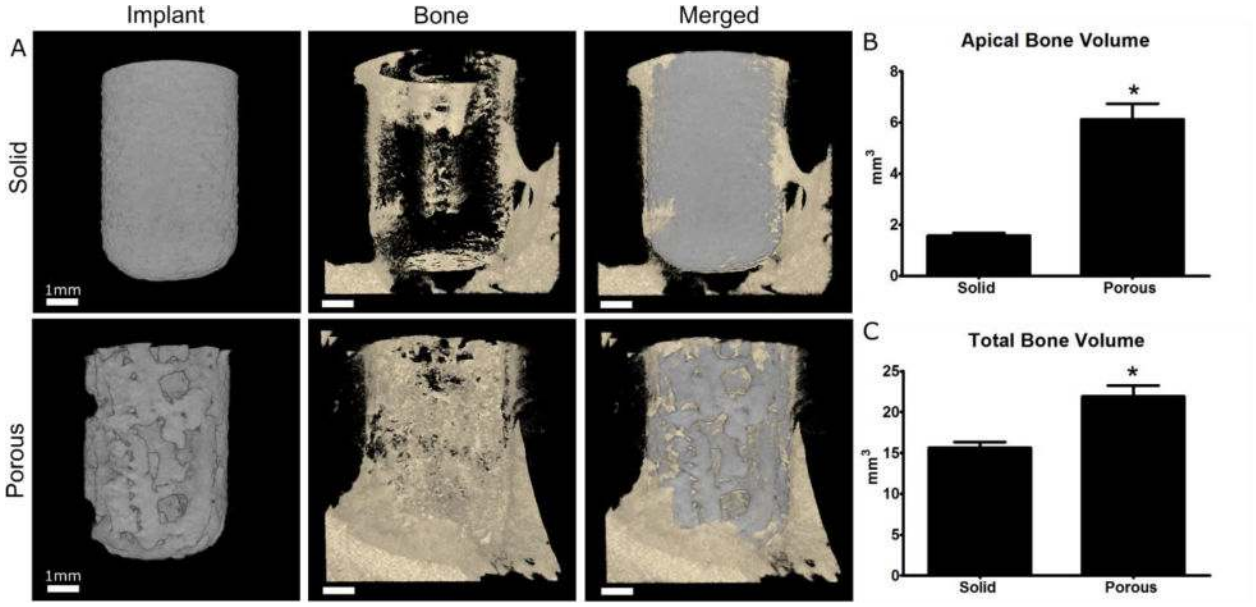

Figure 5.

MicroCT three-dimensional reconstructions of solid and porous implants after 10 weeks in rabbit femurs (A). Total new bone volume within a defined volume of interest including on the lower apical portion of the implant (B) and for the entire implant (C).

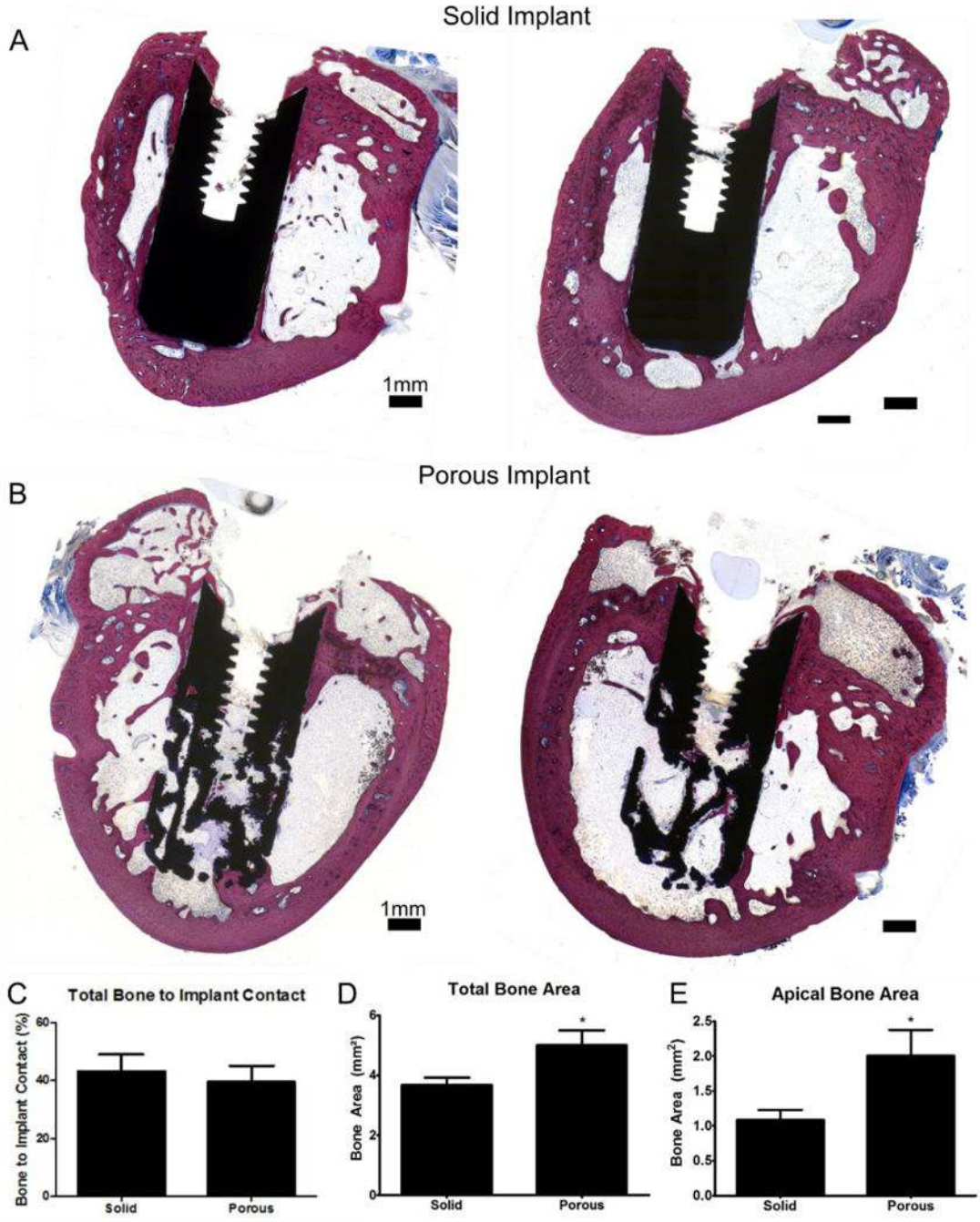

Figure 6.

Histological cross sections of solid (A) and porous implants (B) in rabbit femurs after 10 weeks stained with Stevenel's Blue. Bone to implant contact values along the entire implant (C). Bone area within a defined region of interest encompassing the entire implant (D) and just the apical portion of the implant (E).

Table 1

Surface chemical composition of solid and porous implants obtained from x-ray photoelectron spectroscopy analysis.

Element	Solid	Porous
	Atomic Percent (Average ± Standard Error)	
C	59.3 ± 1.8	56.6 ± 3.1
O	29.9 ± 0.9	29.0 ± 1.9
Ti	3.4 ± 0.4	0.62 ± 0.2
N	3.1 ± 0.5	5.4 ± 0.7
Ca	2.4 ± 0.4	2.7 ± 0.1
Al	1.5 ± 0.7	2.9 ± 0.7
Na	0.2 ± 0.2	1.2 ± 0.2

Table 2

Surface roughness of solid and porous implants obtained from laser confocal microscopy analysis.

Element	Solid	Porous
	Roughness (Average ± Standard Error)	
Ra	2.66 ± 0.03	2.47 ± 0.10
Rz	24.22 ± 0.86	25.72 ± 1.32

Table 3

MicroCT and histological analysis of bone growth in and around solid and porous implants after 10 weeks of implantation in rabbit femora.

		Solid	Porous
		Average ± Standard Error	
MicroCT	Total bone volume	15.6 ± 0.72	21.9 ± 1.3
	Total bone volume/VOI (%)	14.8 ± 0.68	20.7 ± 1.2
	Total bone volume/pore volume (%)	–	46.2 ± 2.7
	Apical bone volume	1.6 ± 0.1	6.1 ± 0.6
	Apical bone volume/VOI (%)	4.6 ± 0.3	17.9 ± 1.8
Histology	Total bone area (mm^2)	3.7 ± 0.2	5.0 ± 0.5
	Total bone area/ROI (%)	16.4 ± 1.0	33.5 ± 4.0
	Total bone to implant contact	43.2 ± 5.8	39.5 ±5.6
	Total bone area/pore area (%)	–	20.1 ± 2.9
	Cortical bone to implant contact	66.8 ± 6.8	55.4 ± 10.0
	Marrow bone to implant contact	37.3 ± 6.9	34.7 ± 6.1
	Apical bone to implant contact	43.9 ± 10.0	44.6 ± 9.5